Neurobiology of Aging 39 (2016) 25–37

Contents lists available at ScienceDirect

Neurobiology of Aging

journal homepage: www.elsevier.com/locate/neuaging

Ketones block amyloid entry and improve cognition in an Alzheimer's model

Jun Xiang Yin [a,1], Marwan Maalouf [a,1], Pengcheng Han [a], Minglei Zhao [b], Ming Gao [c], Turner Dharshaun [c], Christopher Ryan [d], Julian Whitelegge [d], Jie Wu [c], David Eisenberg [b], Eric M. Reiman [e], Felix E. Schweizer [f,**], Jiong Shi [a,*]

[a] Department of Neurology, Barrow Neurological Institute, St. Joseph Hospital and Medical Center, Phoenix, AZ, USA
[b] Department of Biological Chemistry, Molecular Biology Institute, Howard Hughes Medical Institute, UCLA-DOE Institute for Genomics and Proteomics, University of California, Los Angeles, CA, USA
[c] Division of Neurobiology, Barrow Neurological Institute, St. Joseph's Hospital and Medical Center, Phoenix, AZ, USA
[d] The Pasarow Mass Spectrometry Laboratory, NPI-Semel Institute, David Geffen School of Medicine and Brain Research Institute, David Geffen School of medicine, University of California, Los Angeles, CA, USA
[e] Banner Alzheimer's Institute, Phoenix, AZ, USA
[f] Department of Neurobiology, David Geffen School of Medicine, University of California, Los Angeles, CA, USA

ARTICLE INFO

Article history:
Received 3 June 2015
Received in revised form 16 November 2015
Accepted 25 November 2015
Available online 7 December 2015

Keywords:
Ketones
Acetoacetate
β-hydroxybutyrate
Mitochondria
Alzheimer's disease

ABSTRACT

Sporadic Alzheimer's disease (AD) is responsible for 60%–80% of dementia cases, and the most opportune time for preventive intervention is in the earliest stage of its preclinical phase. As traditional mitochondrial energy substrates, ketone bodies (ketones, for short), beta-hydroxybutyrate, and acetoacetate, have been reported to provide symptomatic improvement and disease-modifying activity in epilepsy and neurodegenerative disorders. Recently, ketones are thought as more than just metabolites and also as endogenous factors protecting against AD. In this study, we discovered a novel neuroprotective mechanism of ketones in which they blocked amyloid-β 42, a pathologic hallmark protein of AD, entry into neurons. The suppression of intracellular amyloid-β 42 accumulation rescued mitochondrial complex I activity, reduced oxidative stress, and improved synaptic plasticity. Most importantly, we show that peripheral administration of ketones significantly reduced amyloid burden and greatly improved learning and memory ability in a symptomatic mouse model of AD. These observations provide us insights to understand and to establish a novel therapeutic use of ketones in AD prevention.

1. Introduction

Alzheimer's disease (AD), the most common cause of late-onset dementia, has a high global economic impact (Mayeux and Stern, 2012) and takes an incalculable toll on patients and their families. Remarkable advances in unraveling the biological underpinnings of AD have been made, but little progress in the development of clinical treatments has been achieved (Holtzman et al., 2012). Recent evidence indicates that amyloid-β (Aβ) is absorbed into and transported through distal axons, accumulates to mitochondria of cell bodies, and is further transferred to neighboring neurons (Song et al., 2014). Mitochondrial dysfunction has been associated with the preclinical and clinical stages of AD (Caldeira et al., 2013; Eckert et al., 2012), and an accumulation of Aβ 1–42 causes mitochondrial failure (Calkins et al., 2011). Furthermore, intracellular accumulated Aβ impairs mitochondrial function (Lustbader et al., 2004; Szatmari et al., 2013; Umeda et al., 2011) by binding to mitochondrial proteins (Borger et al., 2011, 2013; Szatmari et al., 2013). Mitochondrial dysfunction increases the formation of reactive oxygen species (ROS), and there is strong evidence linking oxidative stress with AD (Leuner et al., 2012; Lin and Beal, 2006).

Traditionally, beta-hydroxybutyrate (BHB) and acetoacetate (ACA), 2 main ketone bodies that we named ketones, have been regarded as energy carriers (Dedkova and Blatter, 2014). Ketones

This article is dedicated to Nicole Maalouf in memory of her late husband Dr. Marwan Maalouf who was killed by a reckless driver on October 15, 2012.

* Corresponding author at: Department of Neurology, Barrow Neurological Institute, St. Joseph's Hospital and Medical Center, 240 W Thomas Rd, Ste 301, Phoenix, AZ 85013, USA. Tel.: +602 406 4032 (office); fax: (602) 798 0899.
** Corresponding author at: Department of Neurobiology, David Geffen School of Medicine, University of California, CHS 63-323, 650 Charles E. Young Drive South, Los Angeles, CA 90095, USA. Tel.: (310) 794-5733 (office); fax: (310) 825-2224.
E-mail addresses: felixs@ucla.edu (F.E. Schweizer), jiong.shi@dignityhealth.org (J. Shi).
[1] These authors contributed equally to this work.

0197-4580/$ – see front matter © 2016 Elsevier Inc. All rights reserved.
http://dx.doi.org/10.1016/j.neurobiolaging.2015.11.018

are consumed by brain as the major energy sources when glucose is limited (Cunnane et al., 2011; Seyfried and Mukherjee, 2005). As mitochondrial energy substrates, ketones have been reported reducing amyloid neurotoxicity and its pathology, protecting neurons, and improving memory ability (Kashiwaya et al., 2000, 2013; Newport et al., 2015). However, ketones are more than just metabolites (Newman and Verdin, 2014; Shimazu et al., 2013) and are also endogenous neuroprotective factors, but the mechanisms are not understood (Rahman et al., 2014).

We hypothesized that learning and memory deficits in AD could be prevented by ketones through a blockade of amyloid entry into the cell and a reduction of oxidative stress. Our in vitro experimental data showed that ketones prevented oligo-Aβ42–induced membrane disruption, neuronal injury, mitochondrial dysfunction, and ROS formation. Furthermore, ketones reduced intracellular level of Aβ42 and protected synaptic plasticity against oligo-Aβ42 toxicity. In vivo experiments in an AD mouse model revealed that ketones improved mitochondrial function by restoring complex I activity and reducing soluble Aβ42 level. Finally, although ketones did not affect wild-type (WT) animals, they drastically improved memory performance in the AD mouse model. These observations provide a pharmacological foundation for ketones and a new insight on its targets in AD prevention.

2. Materials and methods

2.1. Oligomeric Aβ42 preparation

To prepare soluble oligomeric Aβ42, human synthetic Aβ42 (rPeptide) was treated in 20 μM ammonium acetate in distilled water (pH = 8, ionic strength = 0.25 M), incubated for 30 minutes at room temperature, lyophilized, and stored in −80 °C. The pretreated Aβ42 was dissolved in artificial cerebrospinal fluid (aCSF) or culture media at room temperature immediately before use. The presence and stability of oligomers were tested by electron microscopy and Western blot techniques.

2.2. Animals

All experiments involving animals were done following protocols in accordance to the US Public Health Service's Policy on Humane Care and Use of Laboratory Animals that were approved by the Institutional Animal Care and Use Committee of the Barrow Neurological Institute or University of California, Los Angeles, depending on where experiments were conducted.

APP (PDGFB-APPSwInd; Jackson Laboratory) mice and littermates of B57/Bl6 control mice (12–14 animals per group) were treated with ketones or control saline via daily subcutaneous injections from 4 to 6 months of age. We prepared 10 mL stock solution (0.952 M BHB solution and 0.278 M ACA solution in 0.9% normal saline [NS]). In ketone treatment group, 100 μL/per 20 g mouse body weight (BHB: 600 mg/kg/day, ACA: 150 mg/kg/day) was given, whereas in NS treatment group, 100 μL 0.9% NS per 20 g mouse body weight was given. Precision Xtra blood glucose and ketone monitoring system with precision Xtra blood β-Ketone test strips (Abbott, Alameda, CA, USA) were used for testing ketone concentration. It measures BHB in the capillary whole blood from the mouse tail (Supplementary Fig. 6). Animals were tested behaviorally, euthanized, and the brain tissue was processed for further analysis.

2.3. Primary cultured neurons and hippocampal slices

Primary cortical neurons were prepared from new-born rat or mouse pups according to the standard procedures (Rinetti and Schweizer, 2010) with minor modifications. Cortical neurons were plated on poly-D-lysine–coated glass coverslips in neurobasal media supplemented with 0.5% (wt/vol) L-glutamine, 1% penicillin-streptomycin, 5% fetal bovine serum, and 2% B27 supplement (Invitrogen), and medium was partially replaced every 4 days. On the 14th day, cultured neurons were used for experiments as described in the text.

Coronal hippocampal-entorhinal brain slices of 400 μm were prepared from 1-month-old health Sprague-Dawley rats, ketones treated or no-treated mice. Slices were stored at room temperature in carbogen gas-saturated aCSF (129 mM NaCl, 10 mM glucose, 3 mM KCl, 1.25 mM NaH_2PO_4, 1.8 mM $MgSO_4$, 2 mM $CaCl_2$, and 21 mM $NaHCO_3$, pH 7.4). Slices were then used for various assays as described in the text.

2.4. Negative staining for transmission electron microscopy

Carbon-coated parlodion support films mounted on copper grids were made hydrophilic immediately before use by high-voltage, alternating current glow discharge. Samples of 5 μL were added directly onto grids and allowed to adhere for 3 minutes. Grids were rinsed with 2 drops of distilled water and negatively stained with 1% uranyl acetate for 1 minute. Specimens were examined either in a Hitachi H-7000 electron microscope at an accelerating voltage of 75 kV or an FEI CM120 electron microscope at an accelerating voltage of 120 kV. Images from Hitachi H-7000 were recorded on Kodak electron microscope film 4489 and scanned into digital form. Images from FEI CM120 were recorded digitally by a TIETZ F 224HD CCD camera (2K × 2K).

2.5. Mass spectrometry

Samples were prepared as described earlier and immunoprecipitated with polyclonal antibodies against Aβ 1–40/1–42. Proteins were separated by sodium dodecyl sulfate-polyacrylamide gel electrophoresis, stained with ProteoSilver plus Silver Stain Kit (Sigma), and bands putatively containing Aβ samples were cut out and washed 3 times in a low-retention microcentrifuge tube with 100 μL 25 mM NH_4HCO_3/50% acetonitrile (ACN) before vacuum centrifugation (SpeedVac) to dry. The dried gels were reduced with 10 mM DL-dithiothreitol (DTT; Sigma) for 1 hour at 56 °C and alkylated with 55 mM iodoacetamide (Sigma) for 45 minutes at room temperature in the dark. The gel pieces were washed twice with 25 mM NH_4HCO_3/50% ACN and dried by vacuum centrifugation. Subsequently, 10 μL (20 ng/μL trypsin in 50 mM NH_4HCO_3) trypsin solution was added barely covering the gel pieces to rehydrate the gel pieces on ice for 10 minutes before incubation at 37 °C overnight. On the following day, 40 μL 25 mM NH_4HCO_3/50% ACN was added, agitated for 10 minutes, briefly centrifuged, and the supernatant was collected into a new tube. If necessary, the sample was stored at −80 °C before analysis by nano-liquid chromatography with data-dependent mass spectrometry using an Orbitrap XL (Thermo Scientific, San Jose, CA, USA). Precursor ion-mass measurements (high resolution) and product-ion mass measurements (low resolution) were used to challenge a rat proteome database with the human Aβ precursor sequence added to it using Mascot software (Matrix Science).

2.6. Electrophysiological recordings for synaptic plasticity

Synaptic plasticity was recorded as described previously (Kimura et al., 2012; Maalouf and Rho, 2008). Briefly, field excitatory postsynaptic potentials were evoked every 30 seconds. Recordings were filtered at 2 kHz, digitally sampled at 20 kHz, and the initial slope of the response was measured. After a 30-minute stable baseline, long-term potentiation (LTP) was induced by a theta-burst

protocol (5 times every 15 seconds, 5 bursts spaced 200 ms apart, each burst consisting of 4 pulses at 100 Hz, i.e., 100 pulses total).

2.7. Perforated patch-clamp recordings

We used perforated patch voltage clamp for characterization of the effects of oligo-Aβ42 and ketones in cultured neurons. Briefly, a culture dish placed on the stage of an inverted microscope for visual monitoring was continuously superfused with standard external solution containing the following (in mM): 150 NaCl, 5 KCl, 1 MgCl2, 2 $CaCl_2$, 10 glucose, and 10 HEPES, pH 7.4. Recording electrodes fashioned on a 2-stage pipette puller (3–4 MΩ, P-830; Narishige) were filled with the intracellular solution containing (in mM) 150 KCl, 10 HEPES, 0.2 ethylene glycol tetraacetic acid (EGTA), 2 $MgCl_2$, 4 MgATP, 0.3 NaGTP, and 10 Na_2 phsphocreatine, pH 7.2, supplemented with or without Aβ42 (500 nM) and ketones (1 mM) or Congo red (14 μM). After the patch pipette formed a seal (>2 GΩ), a perforated whole-cell conformation was formed as judged by gradual (5–30 minutes) reduction of the access resistance (to <60 MΩ). Note that the pipette capacitance was not cancelled. The transient limited by the series resistance can be observed as a clear "kink" in the current decay after the voltage step (e.g., Fig. 3C, 6 minutes). The perforation time was scored as 30 minutes if R_a was still ~1 GΩ at 30 minutes. The currents were recorded using a patch-clamp amplifier (200 B; Molecular Devices).

2.8. Intracellular calcium imaging

Intracellular calcium imaging was recorded (Sepulveda et al., 2014). Briefly, primary cultured neurons were loaded with Fluo-3 AM (1 μM, K_d ~335 nM) for 30 minutes. Fluorescent images of neurons were collected at 3-second intervals during a continuous 30-minute period using an LSM 710 confocal microscope while perfusing oligo-Aβ42 (1 μM) with or without ketones (1 mM) in neurobasal medium. Fluorescent signals from different neurons in regions of interest were analyzed using LSM 710 imaging software. Note that the fluorescence values are arbitrary values, and no attempt was made to measure the absolute calcium concentration.

2.9. Measurements of cytotoxicity, oxidation, and mitochondrial function

Cell viability (3-[4,5-dimethylthiazol-2-yl]-2,5-diphenyltetrazolium bromide assays) intracellular ROS measurements using 6-carboxy-2′,7′-dichlorodihydrofluorescein di-acetate (Invitrogen), mitochondrial superoxide determination (Mitosox; Invitrogen), and protein oxidation assays (OxyELISA; Millipore) were performed. Mitochondrial activity was measured from mitochondria isolated from cultured neurons and brain tissue using the MitoXpress fluorescence oxygen probe kit (Luxcel Biosciences) as described previously (Han et al., 2014). Mitochondrial Complex I substrates: 100 mM glutamate and 100 mM malate. Complex II substrates: 100 mM succinate supplemented by 10 μM rotenone.

2.10. ROS levels and protein oxidation measurement

To measure intracellular H_2O_2 levels in the CA1 region, hippocampal slices (400 μm) were incubated with 2 μM 6-carboxy-2′,7′-dichlorodihydrofluorescein di-acetate (Invitrogen) for 30 minutes at room temperature and then transferred to the recording chamber. Slices were equilibrated in the recording chamber for 20 minutes before imaging. Specimens were illuminated using a Lambda LS xenon-arc lamp (Sutter Instrument), a Zeiss filter set 10 (excitation 450–490 nm, beam splitter 510 nm, and emission 515–565 nm), and a ×2.5 0.12NA Zeiss Fluar objective. Fluorescence of the pyramidal layer in CA1 slices was recorded with a CCD camera (UI224x; Imaging Development System, Obersulm, Germany) and analyzed with Image J (Schneider et al., 2012). All measures were normalized to fluorescence in a cell-free area to compensate for fluctuations in background luminosity.

Mitochondrial superoxide levels were assessed in primary cortical cultures using MitoSox Red (Invitrogen). MitoSox Red was initially dissolved in dimethyl sulfoxide and then diluted to 500 μM in HEPES buffer (in mM: NaCl 150, KCl 5, $MgCl_2$ 1, $CaCl_2$ 2, glucose 10, HEPES 10, pH adjusted to 7.4 with NaOH, and final dimethyl sulfoxide concentration ≤0.1%). Neurons were preincubated with MitoSox Red for 30 minutes and then transferred to the recording chamber where they were continuously perfused with HEPES buffer. Imaging was performed with a LSM5 Pascal confocal microscope (Zeiss), and data were analyzed with Image J.

Protein oxidation was measured using the OxyELISA Oxidized Protein Quantitation Kit (Millipore) according to the manufacturer's recommendations. Individual hippocampal slices were incubated with the desired pharmacological agent and homogenized in the provided buffer. Protein concentration was measured with the bicinchoninic acid assay using bovine serum albumin as standard. Protein of 10 μg per sample was used for subsequent analyses. The carbonyl groups in the protein side chains were derivatized to 2,4-dinitrophenylhydrazone (DNP) by reaction with 2,4-dinitrophenylhydrazine. The derivatized proteins were then incubated with a mouse monoclonal antibody (conjugated to horseradish peroxidase) specific to the DNP moiety. Subsequent incubation with the enzyme substrate 3,3′,5,5′-tetramethylbenzidine resulted in a colored product proportional to the degree of protein oxidation. For detection of oxidative protein in brain tissues of APP mice after 2 months of ketone treatment, temporal cortices of mice were dissected and homogenized in RIPA buffer (Sigma) containing 2% 2-mercapethanol. Protein of 20 μg per sample was used to measure protein oxidation with the OxyBlot protein oxidation detection kit (Millipore). DNP-derivatized proteins were separated by 12% polyacrylamide gel electrophoresis followed by Western blotting with a primary antibody against DNP (rabbit anti-DNP antibody). This step was followed by incubation with a secondary antibody conjugated with horseradish peroxidase (goat anti-rabbit immunoglobulin G). Immunoreactive productions were detected by chemiluminescence (Thermo Scientific), and the intensity of blots bands was quantified using the ECL system.

2.11. Behavioral studies

The Morris Water Maze (MWM) was used to test spatial learning and memory function as described previously (Yin et al., 2011) at the end of the 2-month treatment. Mice were given 6 trials per day for 4 days with an intertrial interval of 20 minutes. A single probe trial was carried out 24 hours after the hidden platform task had been completed. Medial temporal lobe and frontal lobe function was assessed using the novel object recognition (NOR) task (Bevins and Besheer, 2006). Twenty-four hours before the NOR task, mice were habituated to the empty open field for 10 minutes. During training, mice were placed in the center of the open field containing 2 identical objects, and the time spent exploring each object during a 5-minute period was quantified. Four hours later, mice were tested by replacing one of the identical objects with a novel object of different shape and color. NOR was quantified using the discrimination index calculated as (exploration time for novel object − exploration time for familiar object)/total exploration time. Rotarod test was used to assess motor performance and to measure the ability of mice to improve motor performance with training. Mice were placed on the elevated accelerating rod (rotarod, 3 cm in diameter; IITC Life Science) beginning at 5 rpm for 4 trials per day

for 2 consecutive days. Each trial lasted a maximum of 10 minutes, during which time the rotating rod underwent a linear acceleration from 5 to 40 rpm over the first 5 minutes of the trial and then remained at maximum speed for the remaining 5 minutes. Animals were scored for their latency (in seconds) to fall (height = 20 cm) for each trial. Animals were rested a minimum of 10 minutes between trials to avoid fatigue.

2.12. Immunostaining

Paraffin-embedded brain sections were immunostained with mouse anti-human Aβ1-16 (6E10; Covance) and visualized using HRP secondary antibodies (Ampli-HRP Kit; Millipore). The following primary antibodies was also used: anti-microtubule-associated protein 2 (EnCor Biotechnology) and anti-HSP 60 (Santa Cruz). Images are maximum-intensity projections for image stacks on LSM 710 confocal microscope.

2.13. Aβ quantification

Total proteins were collected from fresh temporal lobe and hippocampus as described previously (Yin et al., 2014). Samples of fresh temporal lobe cortex and hippocampus were dissected and weighed. Tissue was homogenized and sonicated in 10 volumes of freshly prepared ice-cold Tris-buffered saline (TBS) consisting of 20 mM Tris-HCl (pH 7.4), 137 mM NaCl, and 1× protease inhibitor cocktails (Sigma) with 5 mM (EDTA), and 5 mM EGTA. Brain slices and cultured neurons were washed 3 times for 10 minutes first with medium and then with 0.1 M PBS before being suspended in TBS with protease inhibitors, EDTA, and EGTA. Samples were then homogenized and centrifuged at 90,000 × *g* for 90 minutes (4.0 °C). The supernatant, called TBS extract, was aliquoted and stored at −80 °C until further analysis. The pellets was resuspended and extracted in 88% formic acid (FA), neutralized by addition of 19 volumes of 1 M Tris-base, and centrifuged for 15 minutes at 20,000× g; its supernatant was called FA extract.

Soluble (TBS extract) and insoluble (FA extract) Aβ38, Aβ40, or Aβ42 levels were detected using the immunogenicity assay developed by Meso Scale Discovery (Rockville, MD, USA), specifically the Aβ 3-Plex kit based on the anti-human Aβ 6E10 antibody. APPα and APPβ in TBS extracts were quantified using the sAPPα/sAPPβ multiplex plate. Signals were measured on a SECTOR Imager 6000 reader (Abramowski et al., 2012; Grathwohl et al., 2009; Terwel et al., 2011). As an alternative to the immunogenicity assay, soluble (TBS extract) and insoluble (FA extract) Aβ levels were determined using immunoprecipitation/Western blot protocol (Jin et al., 2009; Mc Donald et al., 2010). Each sample (500 μL) was preincubated with 25 μl Protein A Sepharose (Sigma), gently agitated for 1 hour at 4 °C and centrifuged at 3500 × *g* for 5 minutes. The supernatant was then transferred into a new 1.5-mL tube for immunoprecipitation. Rabbit anti-Aβ 1–40/1–42 polyclonal antibody (Millipore) was added to the supernatant at a ratio of 1:100 and incubated overnight at 4 °C. Protein A Sepharose of 30 μL was added, and the sample was incubated for another 2 hours at 4 °C, washed 3 times with immunoprecipitation wash buffer, and centrifuged at 3500 × *g* for 5 minutes. The supernatant was removed by aspiration. Antigen-antibody-Protein A Sepharose complexes were collected, and 20 μL 2× Tricine sample buffer (Bio-rad) was added and heated in boiling water for 10 minutes, cooled to room temperature, and centrifuged at 15,000 × *g* for 5 minutes. Samples were loaded on 16.5% polyacrylamide Tris-Tricine precast gels (#456-3065; Bio-rad, Hercules, CA, USA) for electrophoresis. Membranes were immunoblotted with 6E10 (1:1000, Covance) at 4 °C overnight and then incubated with the secondary antibody (1:7500, horseradish peroxidase–conjugated anti-mouse IgG; Santa Cruz) for 1 hour at room temperature. Immunoreactive bands were detected by enhanced chemiluminescence (ECL kit; Thermo Scientific) and quantified using ECL system. Aβ42 of 10 ng was used as positive standard sample; TBS was used as a negative control.

2.14. Statistical analysis

Behavioral data from the MWM test were analyzed by 2-way analysis of variance, with groups as the independent between-subject variables, day as within-subject variable, and distance or latency as the dependent variables. Enzyme-linked immunosorbent assay, Western blot, and image analysis data were analyzed where appropriate by Student *t* test or 1-way analysis of variance. Unless indicated otherwise, data are expressed as mean ± standard error of the mean, and $p < 0.05$ was used as statistically significant.

3. Results

3.1. Characterization of oligo-Aβ42

To obtain stable Aβ42 oligomers, synthetic human Aβ42 was solubilized in ammonium acetate, lyophilized, and redissolved in aCSF. Several lines of evidence support the notion that ammonium acetate induced the generation of oligomers. First, electron microscopic analysis revealed different sizes of annular Aβ42 oligomers (Fig. 1A–C, arrows) only when Aβ42 was pretreated with ammonium acetate (Fig. 1A and C). Second, we used Western blot to detect Aβ42 forms. There were monomers, dimers, trimmers, and tetramers in the ammonium acetate samples, but control samples only contained monomers (Fig. 1D and E). Third, size exclusion chromatography was used to corroborate the presence of oligomers. Pure Aβ42 dissolved in aCSF produced a single peak on size exclusion chromatography consistent with monomeric Aβ42. Aβ42 prepared with ammonium acetate produced a peak at the same position as the control sample and another peak consistent with oligo-species (Fig. 1F). Finally, ketones (1 mM, a mixture of 1 mM BHB, and 1 mM ACA) did not affect Aβ42 aggregates (Fig. 1C and F). The neurotoxicity of prepared oligo-Aβ42 was also tested in this study; primary cultured neurons were treated with 1 μM Aβ42 for 24 hours. Compared with nontreated neurons, oligo-Aβ42–treated neurons showed fragmentation of neurites and only approximately half of them survived (0.068 ± 0.006 in oligo-Aβ42 versus 0.144 ± 0.003 in the control, Fig. 1)G–I.

3.2. Effects of oligo-Aβ42 and ketones on synaptic plasticity in vitro

A crucial role for Aβ in causing rapid disruption of synaptic plasticity and memory impairment has been postulated (Klyubin et al., 2012). We tested if ketones could mitigate oligo-Aβ42–induced changes in LTP in the CA1 region of hippocampus. Hippocampal slices were incubated with oligo-Aβ42 with and without pretreatment with ketones. Under control conditions, theta-burst stimulation of the Schaffer collateral fibers led to a large but transient increase in evoked responses (posttetanic potentiation) followed by a smaller but stable, long-lasting increase (LTP) in the amplitude of the CA1 field excitatory postsynaptic potentials (46% ± 5% above baseline 60 minutes after induction). After exposure to oligo-Aβ42 (1 μM) for an hour (45 minutes before and 15 minutes after induction), LTP was completely blocked (Fig. 1J), whereas posttetanic potentiation was unaffected. This result is consistent with the notion that LTP inhibition is one of the most sensitive measures of acute effects of Aβ (Cullen et al., 1997). Surprisingly, pretreatment with ketones for 1 hour before Aβ42 administration restored LTP almost to control levels (36% ± 6% above baseline in field potential amplitude, 78% of control,

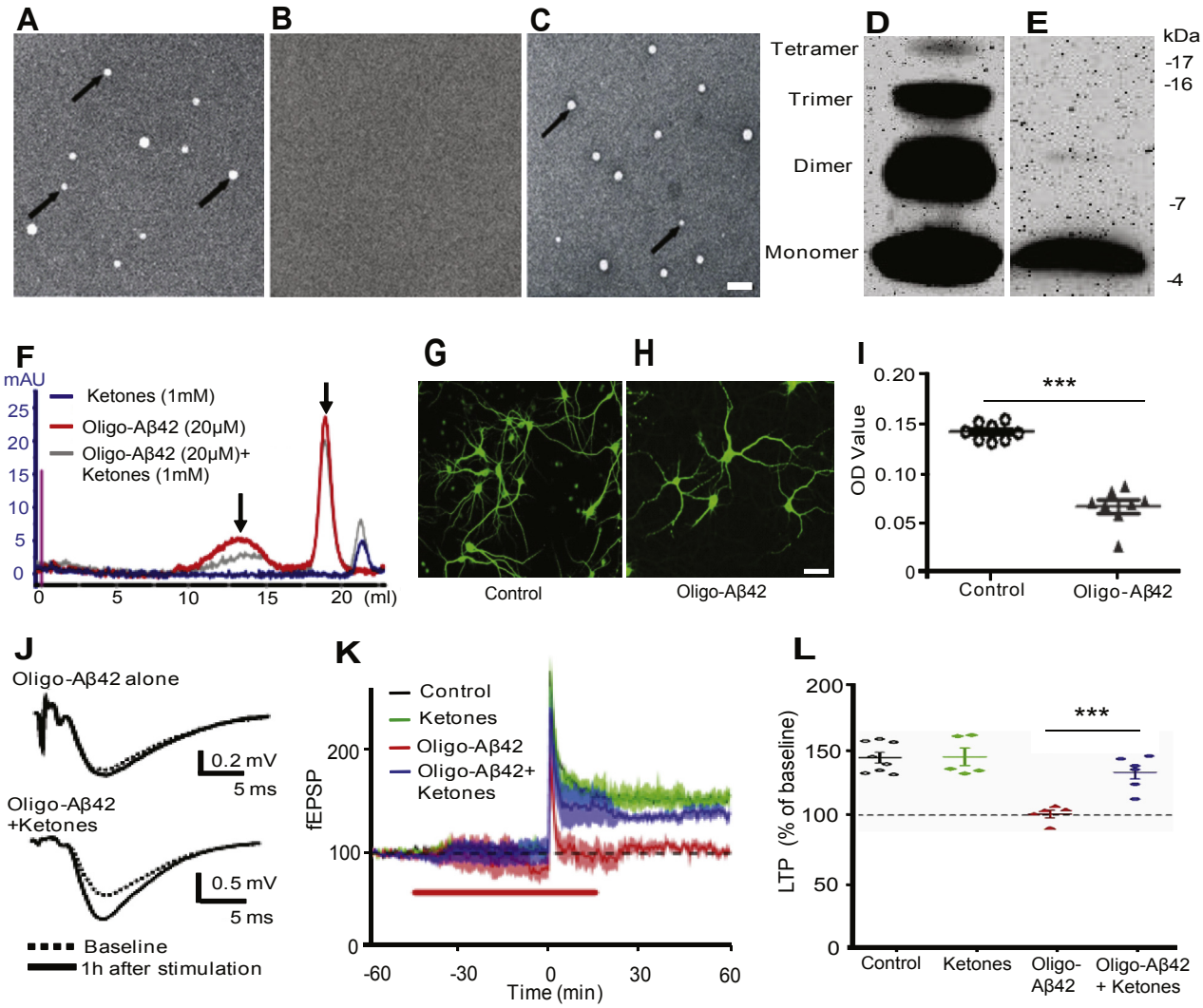

Fig. 1. Characterization of soluble oligo-amyloid-β 42 (Aβ42). Synthetic human Aβ42 was solubilized in ammonium acetate (pH = 8), lyophilized, and redissolved in artificial cerebrospinal fluid (aCSF). Several lines of evidence confirm the generation of oligomers. (A–C) Electron microscopic analysis of oligo-Aβ42. (A) Aβ42 dissolved with ammonium acetate, lyophilized, and suspended in aCSF. Note annular oligomers (arrows). (B) Untreated Aβ42 dissolved in aCSF. No oligomers or fibrils were visible. (C) As in (A) but treated with ketones. No change in the appearance of the oligomers was observed. Scale bar in (C) presents 100 nm. (D and E) Immunoblot of Aβ42 samples was prepared with (D) or without (E) ammonium acetate. Besides monomeric Aβ42, dimer, trimer, and even tetramer forms of Aβ42 were detected after Aβ42 was prepared with ammonium acetate. (F) Size exclusion chromatography analysis: ketones did not affect the molecular weight and, therefore, the structure of Aβ42. Aβ42 prepared with ammonium acetate produced 2 peaks, the monomer peak at 19 mL and a diffuse peak spanning 10–16 mL representing higher molecular weight oligomers with diverse stoichiometry. (G and H) Primary cultured hippocampal neurons were treated for 2 hours without (G) or with (H) oligo-Aβ42 and stained for the neuronal marker microtubule-associated protein 2. Scale bar in (H) presents 100 μM. Note fragmented neurites and fewer surviving neurons in the Aβ42-treated group. (I) The cell viability of neurons was tested using 3-(4,5-dimethylthiazol-2-yl)-2,5-diphenyltetrazolium bromide assay. Oligo-Aβ42 significantly reduced cell viability ($n = 8$, $^{***}p < 0.001$). (J) Examples of field excitatory postsynaptic potentials (fEPSPs) before and after long-term potentiation (LTP) induction from Aβ42-treated slices (top) showed absence of plasticity, whereas ketones could restore LTP (bottom). (K) The slope of the fEPSP was plotted against time for all 4 conditions. Note that Aβ42 virtually abolished LTP, whereas ketone pretreatment restored LTP almost to control levels. (L) Quantification of fEPSP amplitudes 60 minutes after LTP induction revealed an increase above baseline for control slices ($n = 7$), oligo-Aβ42 (1 μM) for 1 hour completely blocked LTP. Pretreatment with ketones for 1 hour before oligo-Aβ42 administration restored LTP ($n = 6$).

Fig. 1J–L), indicating that ketones protected synaptic plasticity from inhibition by oligo-Aβ42.

3.3. *Effects of ketones on intracellular Aβ levels*

To test the possibility of exogenous Aβ42 inhibiting synaptic plasticity through entering into cytoplasm, we treated primary neurons for 2 hours with 1 μM fluorescein-labeled human Aβ42 (rPeptide, Jungbauer et al., 2009). Cells were washed extensively, fixed, and counterstained for Aβ1–16 (6E10, selective for human Aβ42), the mitochondrial protein HSP60, or microtubule-associated protein 2, a neuron-specific marker. Fluorescent Aβ42 aggregates showed different sizes after stained with 6E10 (Fig. 2A–C) and colocalized with the mitochondrial marker HSP60 (Fig. 2D–F). Reconstruction of 3-dimensional volumes (Supplementary Fig. 1A–C) and projection images (Fig. 2)G–I provided strong evidence that human Aβ42 entered the cytoplasm from the extracellular space. To evaluate the level of the internalized Aβ42, neurons treated with oligo-Aβ42 were harvested from culture plates after extensive washing, thus removing any remaining extracellular Aβ42. Western blot analysis showed that the Aβ42 dimer was preferentially present in hippocampal slices and that ketones significantly reduced the level of oligo-Aβ42, specifically dimers (Fig. 2J). Interestingly, we did not see Aβ42 dimers in the monomer Aβ42 treatment group (Fig. 2J). Similar results were obtained when primary cultured neurons were incubated with oligo-Aβ42 or/and ketones (Fig. 2K). Human and

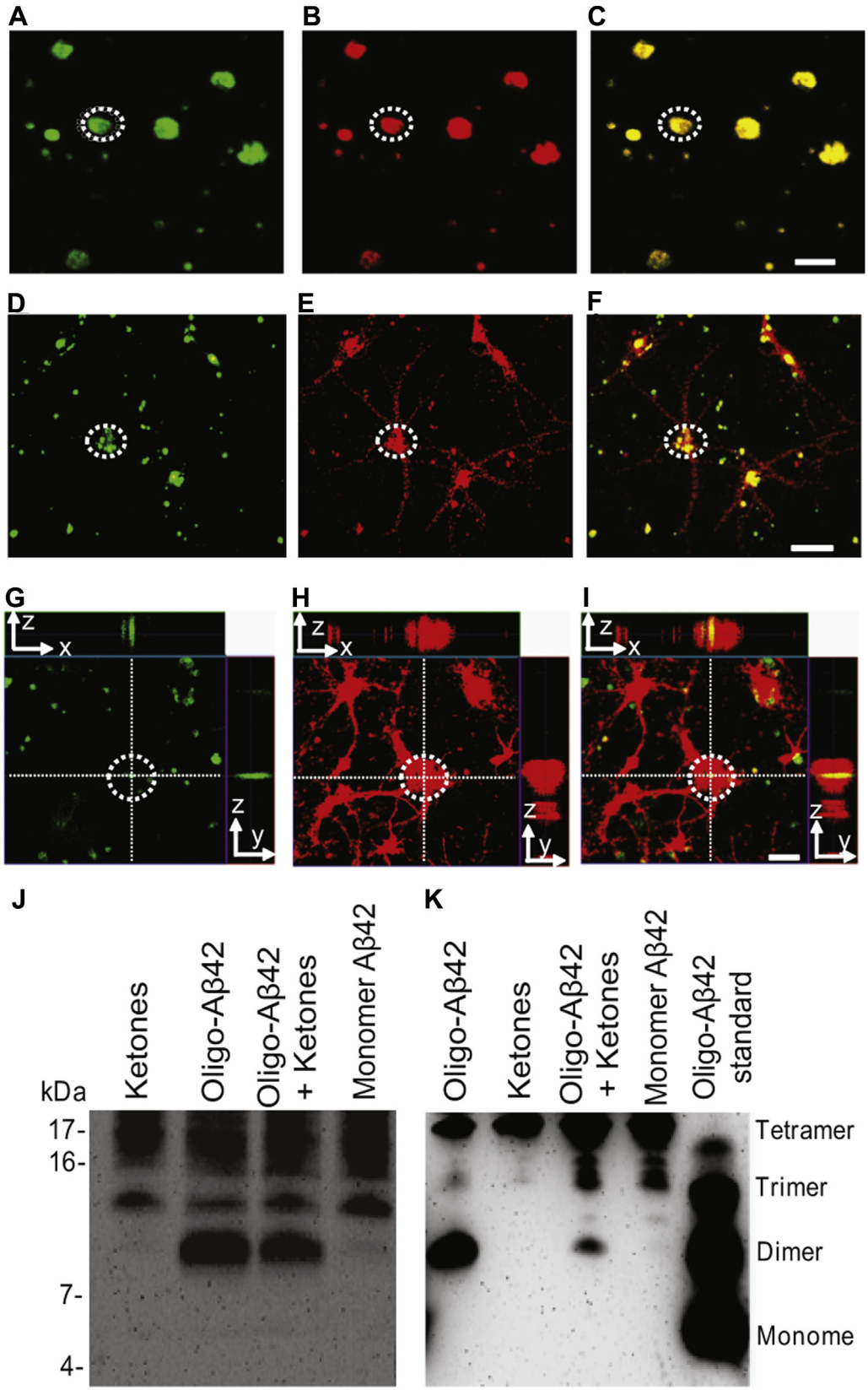

Fig. 2. Internalization of exogenous human amyloid-β 42 (Aβ42) into primary cultured neurons. Primary cultured neurons were incubated with fluorescein labeled Aβ42 (green, 1 μM), and the fluorescent Aβ42 was detected inside cultured neurons. Groups of neurons and hippocampal slices were incubated with exogenous human oligo-Aβ42 (1 μM), and human oligo-Aβ42 was confirmed using Western blot and mass spectrometry. (A) Fluorescein isothiocyanate (FITC)-Aβ42 (green), (B) Aβ antibody 6E10 (red), and (C) merged image, note strong overlap. Scale bar: 10 μm. (D) FITC-Aβ42 (green), (E) mitochondria marker HSP60 (red), and (F) merged image; note colocalization in cell body. Scale bar: 50 μm. (G–I) Large image: single confocal section (x–y) in center of stack. Top image: z–x reconstruction and right image: z–y reconstruction. (G) FITC-Aβ42 (green), (H) microtubule-associated protein 2 (red), and (I) merged image. Scale bar: 20 μm. (J and K) Western blot was used to test Aβ42 levels in hippocampal slices (J) and cultured neurons (K) after slices, and neurons were incubated with oligo-Aβ42 or/and ketones. Ketones reduced the levels of dimers compared with no-ketone controls. (For interpretation of the references to color in this figure legend, the reader is referred to the Web version of this article.)

rodent Aβ42 have slightly different sequences (Supplementary Fig. 2D), and we analyzed the sequences of the Aβ42 dimers by mass spectrometry to ascertain that the Aβ42 dimers originated from the exogenous human oligo-Aβ42 preparation rather than reflecting aggregated rodent Aβ42. Silver staining and Western blotting were used to localize and confirm the human Aβ42 dimer (Supplementary Fig. 2E). As expected, we observed one specific human Aβ42 peptide fragment (Fig. 2C and F) and other nonspecific fragments (Supplementary Fig. S2 E, F). We conclude that human Aβ42 forms the majority of the detected dimers. Soluble oligo-Aβ42 can thus enter the cytoplasm of neurons and be retained mainly as dimers, whereas ketones reduce its intracellular accumulation.

3.4. Effects of ketones on Aβ42-induced perforation activity

It has been proposed that Aβ is able to cause pore formation that allows subsequent calcium entry, which could be involved in neurotoxicity (Kagan et al., 2002; Kotler et al., 2014; Quist et al., 2005; Sepulveda et al., 2014). In addition, small molecule blockers of Aβ channels were identified as candidates for AD therapeutics (Diaz et al., 2009; Fantini et al., 2014; Hirakura et al., 2000; Sepulveda et al., 2014). We found that Aβ42 was taken up by neurons despite the presence of dynasore, a dynamin inhibitor that blocks clathrin-mediated endocytosis (Supplementary Fig. 3A–F). This indicates that a clathrin independent mode of entry, potentially via a pore-forming mechanism. We thus tested the membrane perforation activity induced by oligo-Aβ42 in the absence and presence of ketones. Access resistance (R_a, MΩ) was used for measuring pore formation (Fig. 3A and B) under voltage-clamp conditions (see Materials and methods). The final R_a reached showed no difference among the 4 conditions (Fig. 3B). However, we found that it only took 7.21 ± 0.46 minutes for oligo-Aβ42 (500 nM) in the pipette solution to perforate the membrane to 40 MΩ of R_a (Fig. 3C–E). Simultaneous co-application of ketones (1 mM) and oligo-Aβ42 delayed perforation to 10.73 ± 1.09 minutes (Fig. 3E). When neurons were pretreated with ketones for 2 hours before the recording, perforation was delayed to an average of 22.11 ± 3.14 minutes (Fig. 3E). Noteworthy, this pretreatment delayed perforation beyond 30 minutes for many neurons (full protection). For comparison, we used Congo red that has been shown to antagonize membrane effects of Aβ (Hirakura et al., 2000; Kagan et al., 2012). Congo red delayed perforation induced by Aβ to 25.72 ± 2.43 minutes (Fig. 3E). We next tested whether Aβ42 exposure would trigger an increase in intracellular calcium as expected if Aβ42 has calcium channel properties (Diaz et al., 2009; Quist et al., 2005; Sepulveda et al., 2014). For this, neurons were loaded with the membrane permeable calcium indicator fluo3-AM. Exposure to oligo-Aβ42 alone quickly increased intracellular calcium concentration compared with control (medium alone) (Fig. 3F and Supplementary Fig. 2G–H), whereas ketones again greatly delayed this effect of oligo-Aβ42 (Fig. 3F and G). To investigate whether Aβ42 could enter the cytoplasm through the pores, we included fluorescent fluor-555-Aβ42 (100 μM) inside the patch pipette (Fig. 3H–J). The very high concentration of Aβ42 allowed us to visualize fluorescence inside the neuronal cell body and dendrites after a few minutes. We did not observe any colocalization in the axons and dendrites. It could be because of 2 reasons: (1) this is an acute phase, transportation along the axona/dendrites requires longer incubation time and (2) the concentration of Aβ in axons or dendrites, if any, is much less than that in the soma, far below the detection level. In summary, these data indicate that extracellular Aβ42 can perforate the cell membrane providing direct access to the cytoplasm. Ketones delay perforation and reduce the level of intracellular Aβ42.

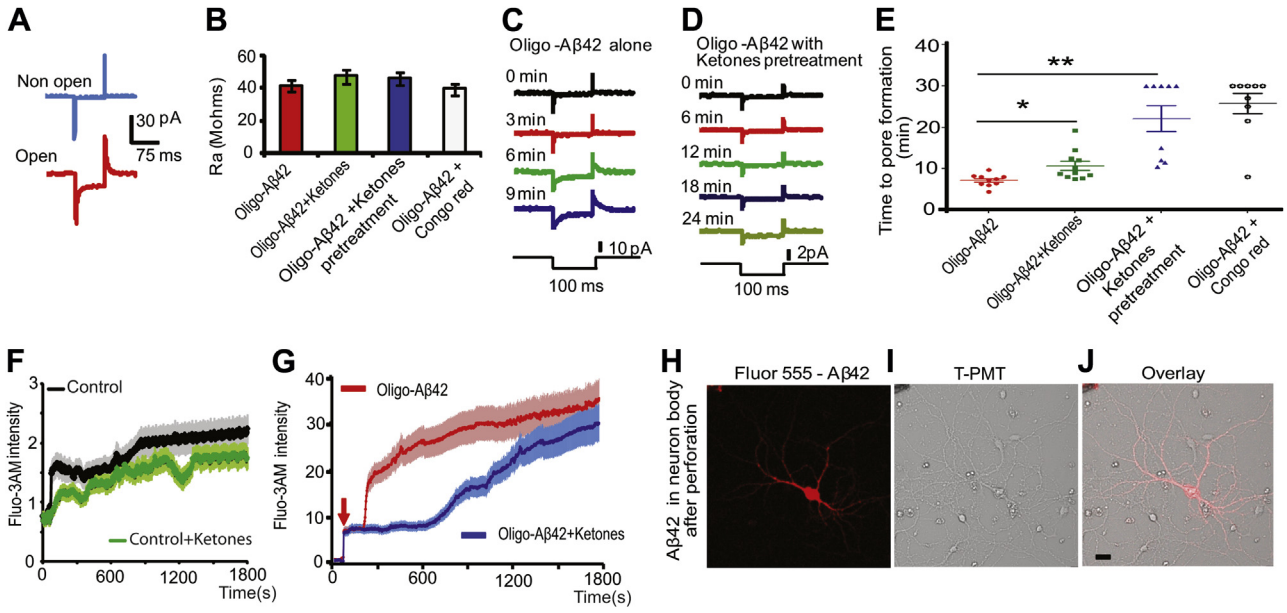

Fig. 3. Effects of ketones on amyloid-β 42 (Aβ42)–induced membrane perforation. Cell attached patch-clamp recordings were performed with Aβ42 alone or together with ketones or Congo red included in the pipette solution. Access resistance, as an indicator of membrane integrity/perforation, was monitored over time and gradually (5–30 minutes) decreased from giga seal to <60 MΩ. (A) Inward current in response to (A) 10 mV, 100 ms voltage step from a holding potential of −70 mV before and after membrane perforation. (B) Access resistance showed no significant difference among these different treatment groups. (C) Intrapipette oligo-Aβ42 (500 nM) alone could perforate the membrane quickly ($n = 10$). (D) This effect was delayed by pretreatment of 1 mM ketones in cultures for 2 hours ($n = 9$, $^{**}p < 0.01$). (E) Summary of perforation time induced by oligo-Aβ42 under different manipulations. The results indicated that internal oligo-Aβ42 (500 nM) along or with co-application of ketones ($n = 11$, $^{*}p < 0.05$) or with pretreatment of ketones. Similar to ketones, Congo red (14 μM) with oligo-Aβ42 (500 nM) in internal solution delayed the perforation time ($n = 9$, $^{**}p < 0.01$). (F and G) Intracellular calcium signal increased dramatically after neurons were treated with oligo-Aβ42 compared with medium alone, whereas ketones decreased intracellular calcium signal. (H and J) Fluor-555-Aβ42 was detected inside the neuron (red signal) after it went from the pipette through the perforated membrane (Fluor-555-Aβ42 concentration: 100 μM, scale bar: 20 μm). (For interpretation of the references to color in this figure legend, the reader is referred to the Web version of this article.)

3.5. Effects of oligo-Aβ42 and ketones on oxidative stress

Mitochondria, the largest source of cellular ROS (Balaban et al., 2005; Murphy, 2009) are a proposed target of Aβ toxicity (Wang et al., 2013). Mitochondrial dysfunction increases formation of ROS (Leuner et al., 2012) causing oxidative stress, which has been implicated in the pathogenesis of AD. Because ketones exhibit antioxidant properties (Shimazu et al., 2013), we tested whether acute oligo-Aβ42 exposure increases ROS levels in hippocampal slices and whether the increase could be minimized by ketones. The fluorescent ROS indicator 6-carboxy-2′,7′-dichlorodihydrofluorescein and an enzyme-linked immunosorbent assay–based test for protein oxidation were used for these experiments. Exposure to oligo-Aβ42 (1 μM) for 2 hours was associated with a 211% ± 40% increase in ROS levels and with a 23% ± 6% increase in protein oxidation relative to control slices. Pretreatment with ketones for 1 hour prevented the effects of oligo-Aβ42: ROS levels (−22% ± 19%) and protein oxidation (−4% ± 6%) did not increase relative to control. Treatment with ketones alone for 2 hours decreased ROS levels and protein oxidation relative to control (Fig. 4A and B). To demonstrate the mitochondrial origin of oligo-Aβ42–induced oxidative stress, we measured superoxide levels in cultured neurons with the mitochondria-specific fluorescent indicator MitoSox Red. Superoxide levels started to increase quickly after application of oligo-Aβ42 and reached 71% ± 20% after 30 minutes relative to baseline, whereas control neurons did not alter the superoxide levels over the same time period (Fig. 4C and Supplementary Fig. 2I–J). Ketones completely blocked the increase in superoxide levels associated with oligo-Aβ42 (Fig. 4C). Ketones thus inhibited oxidative stress by preventing the production of reactive oxygen species, especially mitochondrial derived superoxide, induced by oligo-Aβ42.

3.6. Effects of oligo-Aβ42 and ketones on mitochondrial respiration

To determine more precisely which components of mitochondria were compromised by Aβ42 and whether ketones had the same target, we examined mitochondrial respiration driven by complex I. In healthy rat brain slices, there was no difference in the amplitude relative to baseline between oligo-Aβ42 alone and oligo-Aβ42 + ketones (Fig. 4D and Supplementary Fig. 3A). But oligo-Aβ42 significantly lengthened the T0.5 (time to 50% of the amplitude value that represents mitochondrial respiratory capacity) to 41.8 ± 0.2 minutes, and ketones shortened T0.5 to 15.1 ± 0.1 minutes of complex I (Fig. 4D and Supplementary Fig. 3B). Thus, oligo-Aβ42 acutely impaired mitochondrial complex I, and ketones had a protective effect by restoring mitochondrial function.

3.7. Effects of ketones on oxidized protein and mitochondrial respiration in APP mice

Our data so far suggested that ketones exert a protective effect against acute oligo-Aβ42 exposure. Could ketones also be protective

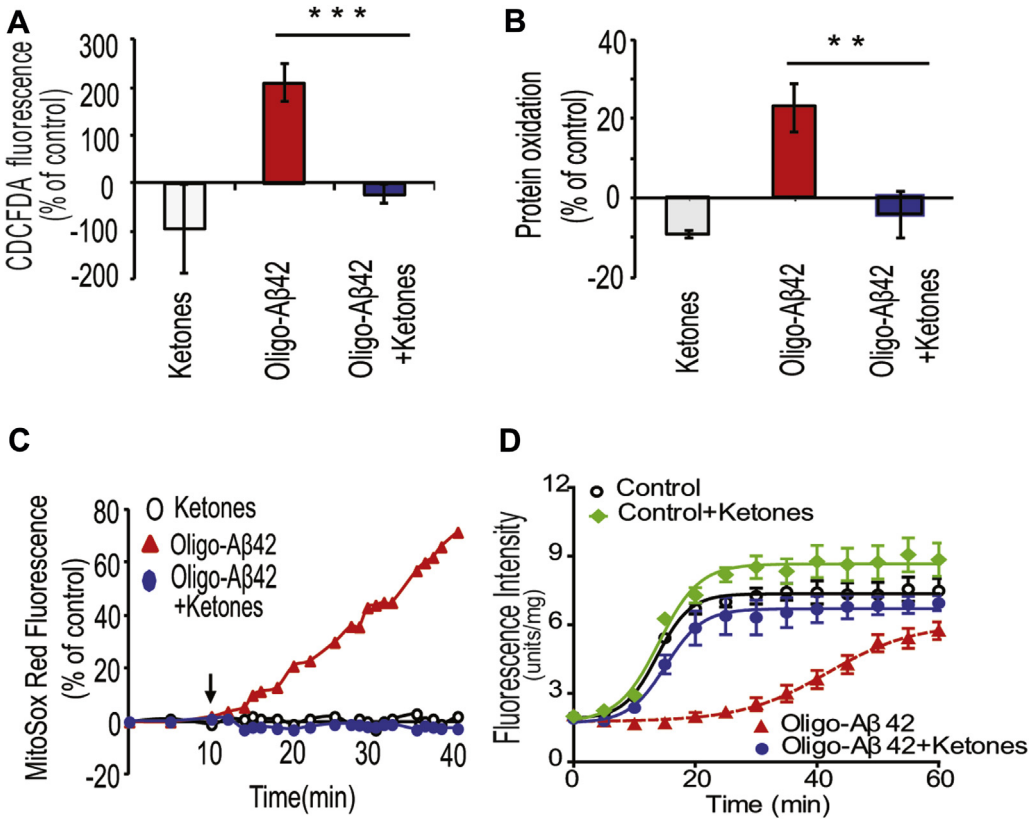

Fig. 4. Effects of oligo-amyloid-β 42 (Aβ42) and ketones on oxidative stress and mitochondrial respiration. Groups of primary cultured neurons or hippocampal slices were treated with olio-Aβ42 or ketones. Reactive oxygen species (ROS) levels, protein oxidation, and mitochondrial respiration were examined. (A) Oligo-Aβ42 significantly increased ROS levels ($n = 10$) in hippocampal slices as measured by the fluorescent ROS indicator. Pretreatment with ketones prevented the oligo-Aβ42–induced increase in ROS levels ($n = 8$, $^{***}p < 0.001$). (B) Ketone treatment decreased protein oxidation ($n = 10$) in hippocampal slices relative to control, and oligo-Aβ42 exposure led to a strong increase in protein oxidation ($n = 16$). Pretreatment with ketones abolished the oligo-Aβ42–induced increase in protein oxidation ($n = 10$, $^{**}p < 0.01$). (C) Oligo-Aβ42 addition (arrow) to primary cortical neurons led to a rapid increase in superoxide levels as indicated by MitoSox Red fluorescence. Ketones blocked the increase in superoxide levels induced by oligo-Aβ42. (D) Mitochondrial complex I function curves were measured in mitochondria isolated from hippocampal slices after acute exposure to oligo-Aβ42. Oligo-Aβ42 (red) reduced complex I function compared with control (black), an effect that could be reversed by ketones (blue). (For interpretation of the references to color in this figure legend, the reader is referred to the Web version of this article.)

in chronic Aβ42 exposure? PDGFB-APPSwInd mice ("APP mice," Hsia et al., 1999; Mucke et al., 2000) were used to address this question. APP mice showed synapses loss, learning deficit starting at 3–4 months and an increase of Aβ plaques at 6 months (Cheng et al., 2004; Roberson et al., 2007). We, therefore, treated 4- to 5-month-old APP mice with daily subcutaneous injections of saline or ketones for 2 months and tested them at 6–7 months of age. Consistently with our in vitro studies, there was significantly high protein oxidation in APP mice brain compared with the WT mice and the level of protein oxidation was decreased to 42.3% ± 3.5% by ketone treatment in APP mice (Fig. 5A and B), indicating that ketones reduced oxidative protein damage in APP mice. We next examined mitochondrial complex I activity in APP animals and found a clear deficit in complex I relative to WT (Fig. 5C–E). A 2-month ketone treatment in APP mice reverses the inhibition of complex I (Fig. 5C–E).

3.8. Effects of ketones on Aβ levels in APP mice brain

Ketones greatly reduced the accumulation of intracellular Aβ42 when primary neurons were exposed to oligo-Aβ42 (Fig. 2). We thus investigated whether ketones also decreased Aβ levels in APP mice. Plaques staining showed fewer plaques were visible through the dentate gyrus of hippocampus of APP + ketone mice (5.1 ± 0.6 plaques per 16×10^4 μm^2) compared with nontreated APP mice (8.3 ± 0.9 plaques per 16×10^4 μm^2) (Fig. 6A and B). We measured both soluble and insoluble Aβ42, Aβ40, and Aβ38 levels after 2 months of ketone treatment. There was no difference in the levels of either soluble or insoluble Aβ38 and Aβ40 (Supplementary Fig. 4A, C, E, and G). However, the levels of soluble and insoluble Aβ42 were lower in APP + ketone mice (soluble: 0.18 ± 0.02 ng/g, insoluble: 29 ± 5 ng/g) compared with nontreated APP mice (soluble: 0.41 ± 0.05 ng/g, insoluble: 51 ± 6 ng/g, Fig. 6C–H). Ketones also increased the ratio of soluble Aβ40/Aβ42 from 2.95 ± 0.38 (APP mice) to 6.78 ± 0.84 (APP + ketone mice) (Supplementary Fig. 4B). But the ratio of insoluble Aβ40/Aβ42 did not change (Supplementary Fig. 4F). The data revealed that ketones decreased the accumulation of Aβ42 and increase the ratio of soluble Aβ40 to Aβ42 in favor of the less toxic Aβ40. Although there was no difference in soluble APPβ between the 2 groups (Supplementary Fig. 4H), ketones increased soluble APPα level (1120 ± 101 versus 911 ± 104 ng/g in APP group, Supplementary Fig. 4D), consistent with a ketone-induced switch to nonamyloidogenic processing of APP. The reduced soluble Aβ42 could thus be because of less Aβ42 production. Western blot analysis of temporal cortex indicated a loss of Aβ42 retained in the brain (Fig. 6E–H) consistent with a decreased Aβ load. Taken together,

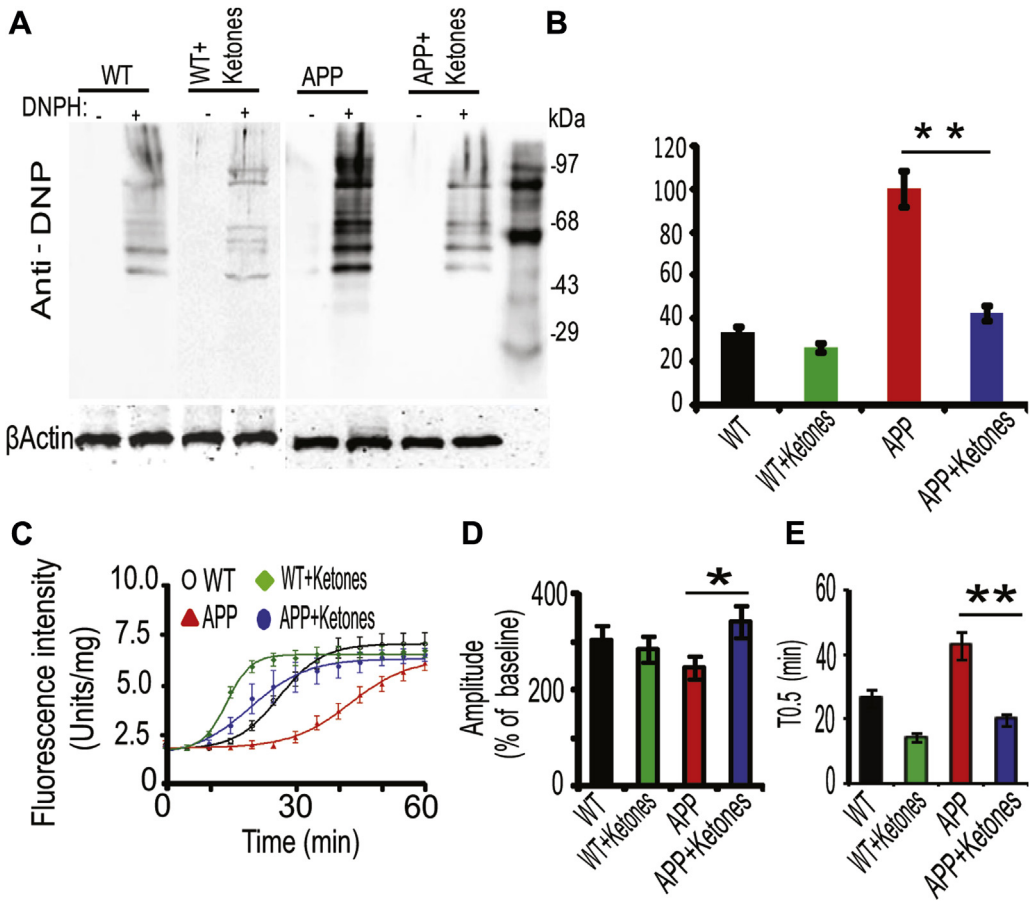

Fig. 5. Effects of ketones on oxidative stress and mitochondrial function in APP mice. APP mice and control wild-type (WT) mice (4–5 months) were treated with daily subcutaneous injections of saline or ketones for 2 months. Brain tissues were collected after sacrifice and oxidative stress level and mitochondrial function in brain tissue were tested. (A and B) Protein oxidation in total 20 μg protein from temporal cortex of APP or WT mice treated for 2 months with saline or ketones. Oxidized proteins were derivatized with 2,4-dinitrophenylhydrazone (DNP) and visualized on Western blots (OxyBlot). The representative samples are shown. Note ketones result in less density of oxidized protein bands. (B) Quantification of protein oxidation: Densitometry was performed on whole lanes shown in (A). Protein oxidation was increased dramatically in APP mice compared with WT mice, whereas protein oxidation was decreased by ketones ($n = 4$, $^{**}p < 0.01$ compared with APP group). (C), (D), and (E) for complex I: mitochondria isolated from the brains of APP animals showed a marked deficit in complex I function compared with control. Ketones increased complex I function of APP animals. Ketone enhanced complex I function of WT animals relative to WT (C). The amplitude percentage relative to baseline was increased in APP + ketone mice compared with APP mice ($^{*}p < 0.05$) (D). The time to 50% amplitude in APP + ketone mice (19.7 ± 1.3 minutes) was shorter than APP mice ($^{**}p < 0.01$) (E).

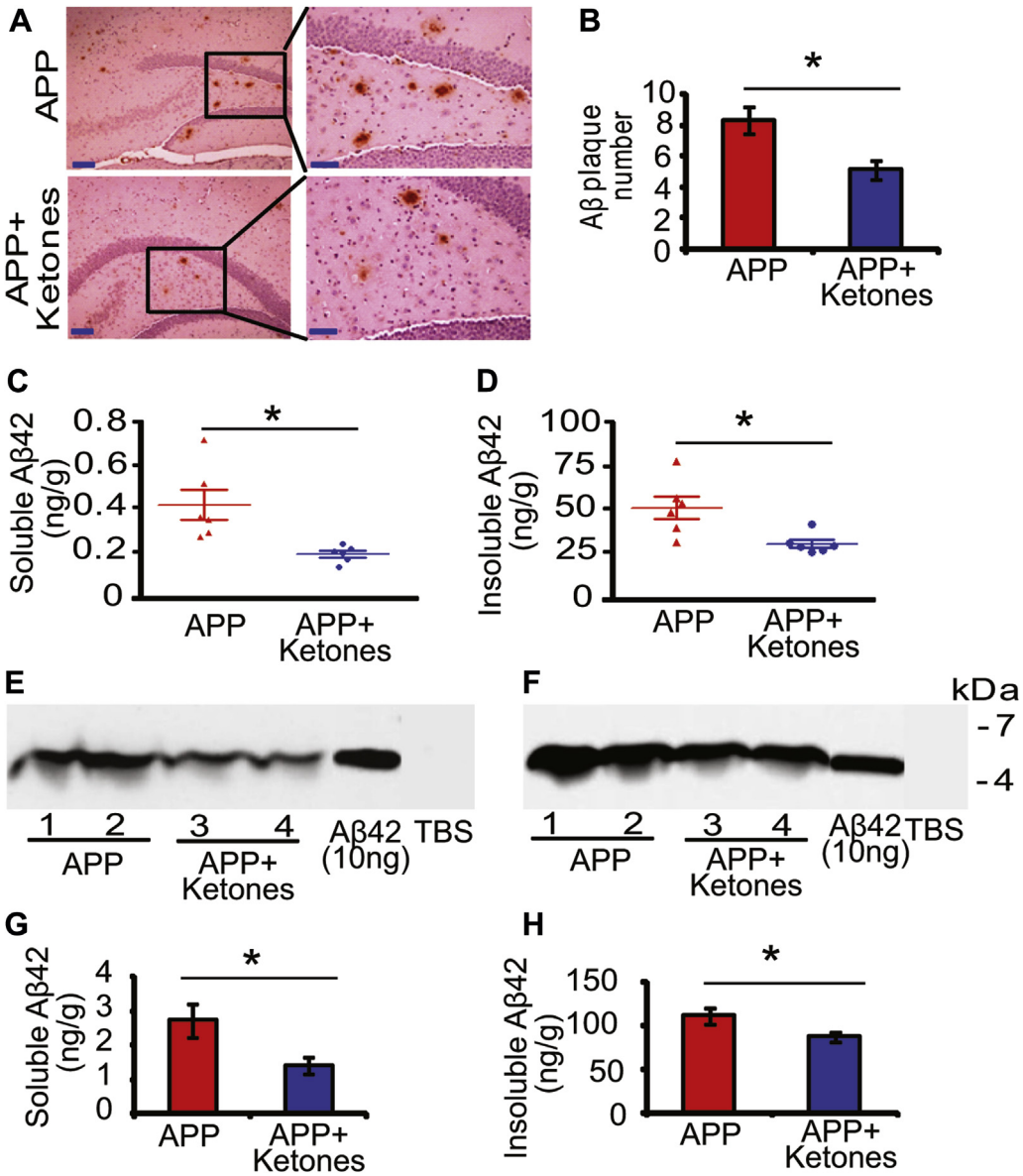

Fig. 6. Effect of ketones on amyloid protein level of APP mice. APP mice (4–5 months) were treated with daily subcutaneous injections of saline or ketones for 2 months. Brain tissues were collected after sacrifice and amyloid level in brain tissue were evaluated through immunohistochemistry staining, Western blot, and enzyme-linked immunosorbent assay (ELISA) methods. (A and B) Amyloid-β (Aβ) plaques were detected in brain sections using the mouse anti-human Aβ antibody (6E10). Two months of ketone treatment significantly reduced the number of Aβ-positive plaques in hippocampal dentate gyrus compared with saline-treated APP mice (A: images. Scale bar left: 200 μm, right: 50 μm. B: quantification of the number of Aβ-positive plaques per 16×10^4 μm^2: APP 8.3 ± 0.9, $n = 6$ mice, APP + ketones 5.1 ± 0.6, $n = 6$ mice, $^*p < 0.05$). (C and D) ELISA was used to test Aβ levels in cortical brain tissues of mice. Brain tissues were homogenized, and the first supernatant was collected (we called Tris-buffered saline "[TBS] extract" containing the soluble amyloid). The pellet was rehomogenized in 88% formic acid (FA) solution, and the second supernatant was collected (we called "FA extract" containing insoluble amyloid). The amount of Aβ42 was quantified by a sandwich immunoassay on Meso Scale Discovery plates. (C) Ketones decreased soluble Aβ42 compared with the control APP group ($^*p < 0.05$). (D) Ketones also reduced the level of insoluble Aβ42 compared with the control APP group ($n = 6$–7 per group, $^*p < 0.05$). The levels of Aβ40, Aβ38, soluble APPα, and soluble APPβ were seen in Supplementary Fig. 4. (E–H) TBS extract and FM extract were immunoprecipitated with Aβ40/42 antibody, followed by Western blot using antibody 6E10. Western blot and analysis data were shown in (E) and (G) (TBS extract) and (F and H) (FA extract); Aβ42 (10 ng) was used as positive control. $^*p < 0.05$, $n = 6$ mice per group.

these data suggest that ketones strongly reduce the levels of Aβ42 in APP mice brain.

3.9. Effect of ketones on synaptic plasticity, behavior, and cognitive performance of APP mice

To understand the effects of ketones on learning and memory, we tested the behavior and cognitive performance of mice, the synaptic plasticity in hippocampus from mice after treating with ketones for 2 months. In the MWM test, the rate of learning was similar in all groups (Fig. 7A and B). During the 4-day period of learning, the escape latency and swimming distance of ketone-treated mice were shorter relative to nontreated mice of the same genotype (WT and APP, Fig. 7A and B). All groups showed similar swim speeds (Supplementary Fig. 5A). During the probe trial (Supplementary Fig. 5B), the time spent in the target quadrant (Fig. 7C) and the numbers of platform crossings (Fig. 7D) were measured. WT and WT + ketone animals performed at very similar levels. APP mice spent less time in target quadrant (10.5 ± 1.5 seconds, $n = 12$ versus 15.0 ± 2.4 seconds, $n = 13$ in APP + ketones, $^*p < 0.05$) and rarely crossed the original platform location (2.14 ± 0.32 versus 4.78 ± 0.49 in APP + ketones, $^*p < 0.05$),

indicating that they did not remember the platform location. APP + ketone mice performed similar to WT and much better than APP mice (Fig. 7C and D). Rotarod performance (Supplementary Fig. 5C and D) and swim speeds in water maze supported that the cognitive difference observed were not because of motor ability. We also tested the effect of ketones on nonspatial memory performance using the NOR test (Supplementary Fig. 5E). The NOR test is commonly used to assess working memory related to frontal cortex and medial temporal lobe (Bevins and Besheer, 2006; Dere et al., 2007; Harris et al., 2010). Again, ketones significantly improved the performance of APP mice: more time was spent with novel objects (26.3% ± 5.8%, $n = 12$) compared with APP mice (12.5% ± 3.6%, $n = 14$, $p < 0.05$) (Fig. 7E and F). To examine the effect of ketones on the synaptic plasticity, we recorded LTP using hippocampal slices from these 4 groups. We did not find significant difference in LTP between WT mice and WT + ketone mice (Fig. 7G and H). In APP transgenic mice, ketone treatment significantly increased LTP (166.9% ± 11.8% above baseline versus 144.1% ± 3.9 % in nontreated APP mice, Fig. 7I and J). This result is consistent with our in vitro LTP test where ketones protected synaptic plasticity from depression by acute exposure to Aβ42 (Fig. 1J–L). Taken together, these behavioral tests indicated that ketones improved cognitive performance in APP mouse, even when treatment was started at the onset of cognitive deficits.

4. Discussion

In this study, we addressed the question whether ketones could alleviate acute and chronic deficits in models of AD. After acute exposure to exogenous oligo-Aβ42, we found intracellular exogenous Aβ42 level increased, stronger oxidative stress, mitochondrial complex I dysfunction, and inhibition of long-term plasticity in hippocampal slices. Pre-exposure of the cells or brain slices to ketones blocked oligo-Aβ42 entry and protected against its neurotoxicity. This “acute exposure” model might allow for determining the acute effects of Aβ42 without compensation at the cellular level. The time course of AD is not a monotonic decline, but progression occurs in spurts of dysfunction interspersed with periods of

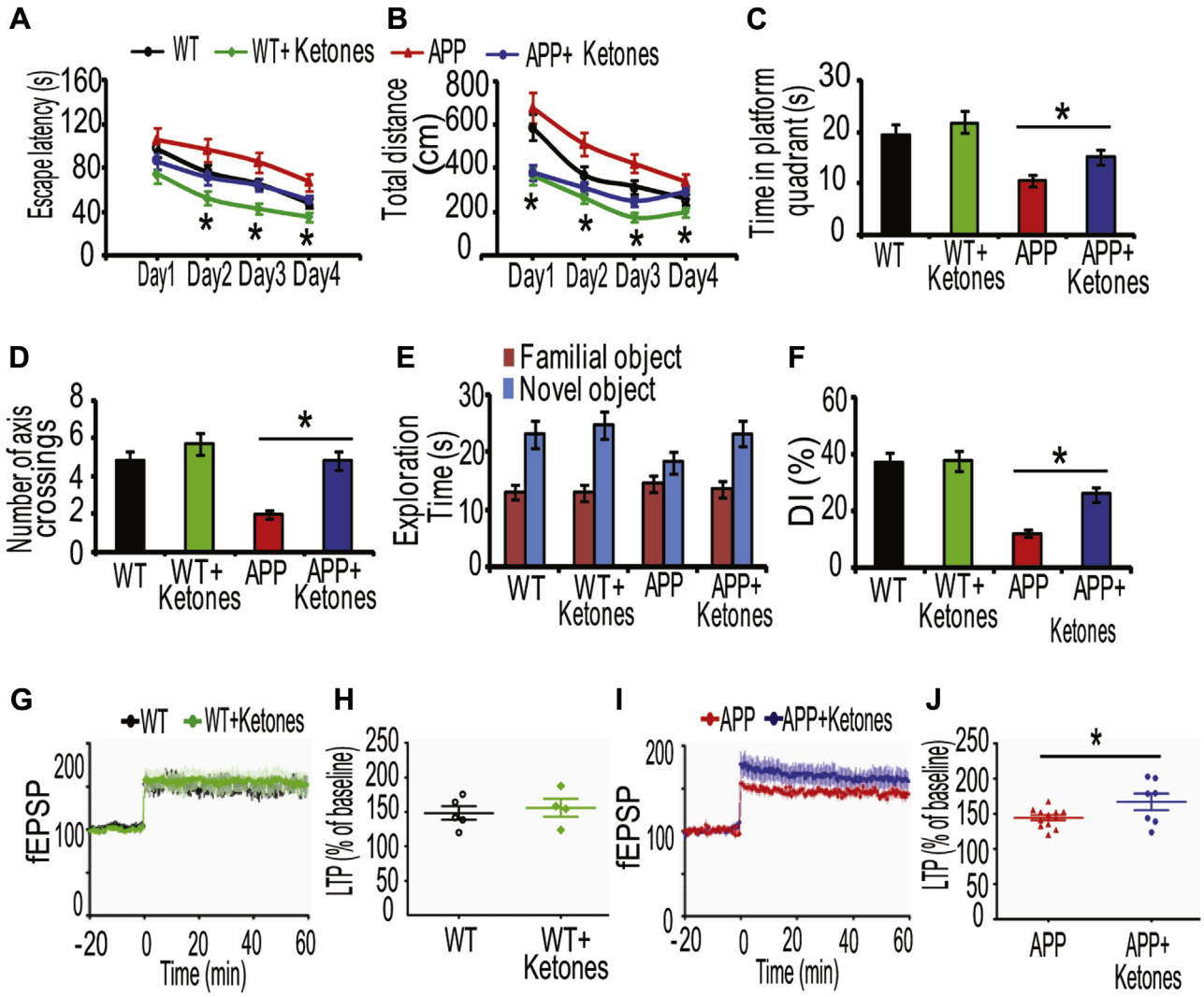

Fig. 7. Effects of ketones on cognitive performance and hippocampal synaptic plasticity of APP mice. APP mice and wild-type (WT) mice (4–5 months old) were treated with daily subcutaneous injections of saline or ketones for 2 months. The memory and cognitive ability of all mice were tested before sacrifice. (A–D) Data from Morris Water Maze test. Escape latency (A) and total distance (B) in learning trials. Data showed ketones boosted the performance in APP mice. (C and D) Data from the probe memory test after platform was removed. Ketones improved the time spent in platform quadrant (C), and number of crossings over where the platform was placed (D) in APP mice. (E–F) Data from novel object recognition test. The exploration time (seconds) of familiar and novel object (E) and the discrimination index (DI) (F). Ketones significantly improved the DI of APP mice ($n = 12$–14 mice/per group, $^*p < 0.05$). (G and H) Long-term potentiation (LTP) was examined in hippocampal slices. There was no significant difference in LTP between WT and WT + ketone mice (G and H). Relative to baseline, LTP was increased more in APP + ketone mice ($n = 7$ slices from 4 mice) than in APP mice ($n = 12$ slices from 5 mice, $^*p < 0.05$) (I and J).

apparent recovery that might be because of changes in Aβ42 load. Our in vitro model reflects potentially rapid increases in cerebral Aβ42 levels during network dysfunction (Mucke and Selkoe, 2012). Elevated ketone levels could protect against further deterioration during disease spurts by inhibiting Aβ42-induced perforation activity.

To address whether ketones can be effective in alleviating symptoms because of chronic aspects of AD, we chose a mouse model overexpressing human APP (Hsia et al., 1999). This mouse line has been shown to exhibit pathologic markers and cognitive deficits reminiscent of AD before 4 months of age (Harris et al., 2010; Mucke et al., 2000; Pujadas et al., 2014). We thus chose 4 months as the start point of treatment because at this age, mice are symptomatic, potentially reflecting an early clinical stage of AD. After 2 months of saline treatment, APP animals showed severe deficits relative to WT mice in synaptic plasticity and cognitive performance, whereas motor function remained unaffected. We also observed plaque formation in hippocampus, especially dentate gyrus, an increase in oxidized proteins, and a strong deficit in mitochondrial complex I function.

APP mice treated for 2 months with ketones showed few signs of the deficits found in saline-treated control APP mice: mitochondrial complex I function was restored, the number of plaques was vastly reduced, and the cognitive function was increased close to control levels. This remarkable result is even more encouraging because none of these metrics were influenced by ketones in WT animals; it is unlikely that ketones simply boosted an alternative pathway that allowed the system to circumnavigate the Aβ42-dependent deficits. Two- to 3-month-old APP animals do show clear deficits relative to WT controls (Harris et al., 2010) and whereas the performance is slightly better in the NOR task at the younger age, our 6-month-old ketone-treated animals perform almost at WT levels and considerably better than at 2–3 months (Fig. 4 in Harris et al., 2010). We thus conclude that ketones not only slowed but also reversed at least some of the symptoms. The underlying cause of the disease, here the APP overexpression, is of course not affected by ketones, and it seems likely that continued ketone treatment is necessary to retain the savings at later ages. But we note that ketones reduced the levels of Aβ42 and also increased soluble APPα, which is produced by α-secretase cleavage of APP and is not associated with amyloid formation. Soluble βAPP, Aβ40, and Aβ38 were not affected by ketones indicating that ketones' effects changed in APP processing in addition to decreasing Aβ42 levels. Such altered processing might produce savings even after ketone treatment is suspended.

Ketones are naturally produced in response to starvation when fat, rather than glucose becomes the primary source of energy. "Ketogenic diets" have been used to treat epilepsy in children since the 1920s (Dhamija et al., 2013). The usefulness of ketogenic diets to manage AD, Parkinson's disease, traumatic brain injury, and stroke has received increasing attention in recent years. In humans with mild cognitive impairment, a low-carbohydrate diet produced cognitive improvement relative to a high-carbohydrate control group (Krikorian et al., 2012). However, ketogenic diets show low compliance and side effects (Payne et al., 2011) that limit their use in the long-term management of degenerative diseases, especially in the elderly. Food additives that aim to increase endogenous ketone production have been developed and show some promise in the treatment of AD (Thaipisuttikul and Galvin, 2012). Our study indicates that peripheral delivery of ketones through daily subcutaneous injections can be sufficient to reverse cognitive decline. This makes ketones and their cellular interactors genuine and exciting treatment targets for neurodegenerative diseases.

Taken together, ketones improved synaptic plasticity and cognitive performance in Aβ-induced pathogenesis of AD model by blocking intracellular Aβ42 accumulation, enhancing mitochondrial complex I activity, and reducing oxidative stress. These findings provide a foundation for the use of ketones and their molecular targets in symptomatic, potentially causal treatment of AD.

Disclosure statement

The authors report no conflict of interest.

Acknowledgements

This work is supported by the Mary S. Easton Center for Alzheimer's Disease Research at UCLA, the Arizona Alzheimer's Disease Consortium AG019610 to EMR, and the Barrow Neurological Foundation BNF 3031880 to JS.

Appendix A. Supplementary data

Supplementary data related to this article can be found, in the online version, at http://dx.doi.org/10.1016/j.neurobiolaging.2015.11.018.

References

Abramowski, D., Rabe, S., Upadhaya, A.R., Reichwald, J., Danner, S., Staab, D., Capetillo-Zarate, E., Yamaguchi, H., Saido, T.C., Wiederhold, K.H., Thal, D.R., Staufenbiel, M., 2012. Transgenic expression of intraneuronal Abeta42 but not Abeta40 leads to cellular Abeta lesions, degeneration, and functional impairment without typical Alzheimer's disease pathology. J. Neurosci. 32, 1273–1283.

Balaban, R.S., Nemoto, S., Finkel, T., 2005. Mitochondria, oxidants, and aging. Cell 120, 483–495.

Bevins, R.A., Besheer, J., 2006. Object recognition in rats and mice: a one-trial non-matching-to-sample learning task to study 'recognition memory'. Nat. Protoc. 1, 1306–1311.

Borger, E., Aitken, L., Du, H., Zhang, W., Gunn-Moore, F.J., Yan, S.S., 2013. Is amyloid binding alcohol dehydrogenase a drug target for treating Alzheimer's disease? Curr. Alzheimer Res. 10, 21–29.

Borger, E., Aitken, L., Muirhead, K.E., Allen, Z.E., Ainge, J.A., Conway, S.J., Gunn-Moore, F.J., 2011. Mitochondrial beta-amyloid in Alzheimer's disease. Biochem. Soc. Trans. 39, 868–873.

Caldeira, G.L., Ferreira, I.L., Rego, A.C., 2013. Impaired transcription in Alzheimer's disease: key role in mitochondrial dysfunction and oxidative stress. J. Alzheimers Dis. 34, 115–131.

Calkins, M.J., Manczak, M., Mao, P., Shirendeb, U., Reddy, P.H., 2011. Impaired mitochondrial biogenesis, defective axonal transport of mitochondria, abnormal mitochondrial dynamics and synaptic degeneration in a mouse model of Alzheimer's disease. Hum. Mol. Genet. 20, 4515–4529.

Cheng, I.H., Palop, J.J., Esposito, L.A., Bien-Ly, N., Yan, F., Mucke, L., 2004. Aggressive amyloidosis in mice expressing human amyloid peptides with the Arctic mutation. Nat. Med. 10, 1190–1192.

Cullen, W.K., Suh, Y.H., Anwyl, R., Rowan, M.J., 1997. Block of LTP in rat hippocampus in vivo by beta-amyloid precursor protein fragments. Neuroreport 8, 3213–3217.

Cunnane, S., Nugent, S., Roy, M., Courchesne-Loyer, A., Croteau, E., Tremblay, S., Castellano, A., Pifferi, F., Bocti, C., Paquet, N., Begdouri, H., Bentourkia, M., Turcotte, E., Allard, M., Barberger-Gateau, P., Fulop, T., Rapoport, S.I., 2011. Brain fuel metabolism, aging, and Alzheimer's disease. Nutrition 27, 3–20.

Dedkova, E.N., Blatter, L.A., 2014. Role of beta-hydroxybutyrate, its polymer poly-beta-hydroxybutyrate and inorganic polyphosphate in mammalian health and disease. Front. Physiol. 5, 260.

Dere, E., Huston, J.P., De Souza Silva, M.A., 2007. The pharmacology, neuroanatomy and neurogenetics of one-trial object recognition in rodents. Neurosci. Biobehav. Rev. 31, 673–704.

Dhamija, R., Eckert, S., Wirrell, E., 2013. Ketogenic diet. Can J. Neurol. Sci. 40, 158–167.

Diaz, J.C., Simakova, O., Jacobson, K.A., Arispe, N., Pollard, H.B., 2009. Small molecule blockers of the Alzheimer Abeta calcium channel potently protect neurons from Abeta cytotoxicity. Proc. Natl. Acad. Sci. U. S. A. 106, 3348–3353.

Eckert, G.P., Renner, K., Eckert, S.H., Eckmann, J., Hagl, S., Abdel-Kader, R.M., Kurz, C., Leuner, K., Muller, W.E., 2012. Mitochondrial dysfunction—a pharmacological target in Alzheimer's disease. Mol. Neurobiol. 46, 136–150.

Fantini, J., Di Scala, C., Yahi, N., Troadec, J.D., Sadelli, K., Chahinian, H., Garmy, N., 2014. Bexarotene blocks calcium-permeable ion channels formed by neurotoxic Alzheimer's beta-amyloid peptides. ACS Chem. Neurosci. 5, 216–224.

Grathwohl, S.A., Kalin, R.E., Bolmont, T., Prokop, S., Winkelmann, G., Kaeser, S.A., Odenthal, J., Radde, R., Eldh, T., Gandy, S., Aguzzi, A., Staufenbiel, M., Mathews, P.M., Wolburg, H., Heppner, F.L., Jucker, M., 2009. Formation and maintenance of Alzheimer's disease beta-amyloid plaques in the absence of microglia. Nat. Neurosci. 12, 1361–1363.

Han, P., Tang, Z., Yin, J., Maalouf, M., Beach, T.G., Reiman, E.M., Shi, J., 2014. Pituitary adenylate cyclase-activating polypeptide protects against beta-amyloid toxicity. Neurobiol. Aging 35, 2064–2071.
Harris, J.A., Devidze, N., Halabisky, B., Lo, I., Thwin, M.T., Yu, G.Q., Bredesen, D.E., Masliah, E., Mucke, L., 2010. Many neuronal and behavioral impairments in transgenic mouse models of Alzheimer's disease are independent of caspase cleavage of the amyloid precursor protein. J. Neurosci. 30, 372–381.
Hirakura, Y., Yiu, W.W., Yamamoto, A., Kagan, B.L., 2000. Amyloid peptide channels: blockade by zinc and inhibition by Congo red (amyloid channel block). Amyloid 7, 194–199.
Holtzman, D.M., Mandelkow, E., Selkoe, D.J., 2012. Alzheimer disease in 2020. Cold Spring Harbor Perspect. Med. 2, a011585.
Hsia, A.Y., Masliah, E., McConlogue, L., Yu, G.Q., Tatsuno, G., Hu, K., Kholodenko, D., Malenka, R.C., Nicoll, R.A., Mucke, L., 1999. Plaque-independent disruption of neural circuits in Alzheimer's disease mouse models. Proc. Natl. Acad. Sci. U. S. A. 96, 3228–3233.
Jin, L., Galonek, H., Israelian, K., Choy, W., Morrison, M., Xia, Y., Wang, X., Xu, Y., Yang, Y., Smith, J.J., Hoffmann, E., Carney, D.P., Perni, R.B., Jirousek, M.R., Bemis, J.E., Milne, J.C., Sinclair, D.A., Westphal, C.H., 2009. Biochemical characterization, localization, and tissue distribution of the longer form of mouse SIRT3. Protein Sci. 18, 514–525.
Jungbauer, L.M., Yu, C., Laxton, K.J., LaDu, M.J., 2009. Preparation of fluorescently-labeled amyloid-beta peptide assemblies: the effect of fluorophore conjugation on structure and function. J. Mol. Recognit. 22, 403–413.
Kagan, B.L., Hirakura, Y., Azimov, R., Azimova, R., Lin, M.C., 2002. The channel hypothesis of Alzheimer's disease: current status. Peptides 23, 1311–1315.
Kagan, B.L., Jang, H., Capone, R., Teran Arce, F., Ramachandran, S., Lal, R., Nussinov, R., 2012. Antimicrobial properties of amyloid peptides. Mol. Pharm. 9, 708–717.
Kashiwaya, Y., Bergman, C., Lee, J.H., Wan, R., King, M.T., Mughal, M.R., Okun, E., Clarke, K., Mattson, M.P., Veech, R.L., 2013. A ketone ester diet exhibits anxiolytic and cognition-sparing properties, and lessens amyloid and tau pathologies in a mouse model of Alzheimer's disease. Neurobiol. Aging 34, 1530–1539.
Kashiwaya, Y., Takeshima, T., Mori, N., Nakashima, K., Clarke, K., Veech, R.L., 2000. D-beta-hydroxybutyrate protects neurons in models of Alzheimer's and Parkinson's disease. Proc. Natl. Acad. Sci. U. S. A. 97, 5440–5444.
Kimura, R., Ma, L.Y., Wu, C., Turner, D., Shen, J.X., Ellsworth, K., Wakui, M., Maalouf, M., Wu, J., 2012. Acute exposure to the mitochondrial complex I toxin rotenone impairs synaptic long-term potentiation in rat hippocampal slices. CNS Neurosci. Ther. 18, 641–646.
Klyubin, I., Cullen, W.K., Hu, N.W., Rowan, M.J., 2012. Alzheimer's disease Abeta assemblies mediating rapid disruption of synaptic plasticity and memory. Mol. Brain 5, 25.
Kotler, S.A., Walsh, P., Brender, J.R., Ramamoorthy, A., 2014. Differences between amyloid-beta aggregation in solution and on the membrane: insights into elucidation of the mechanistic details of Alzheimer's disease. Chem. Soc. Rev. 43, 6692–6700.
Krikorian, R., Shidler, M.D., Dangelo, K., Couch, S.C., Benoit, S.C., Clegg, D.J., 2012. Dietary ketosis enhances memory in mild cognitive impairment. Neurobiol. Aging 33, 425.e19–425.e27.
Leuner, K., Muller, W.E., Reichert, A.S., 2012. From mitochondrial dysfunction to amyloid beta formation: novel insights into the pathogenesis of Alzheimer's disease. Mol. Neurobiol. 46, 186–193.
Lin, M.T., Beal, M.F., 2006. Mitochondrial dysfunction and oxidative stress in neurodegenerative diseases. Nature 443, 787–795.
Lustbader, J.W., Cirilli, M., Lin, C., Xu, H.W., Takuma, K., Wang, N., Caspersen, C., Chen, X., Pollak, S., Chaney, M., Trinchese, F., Liu, S., Gunn-Moore, F., Lue, L.F., Walker, D.G., Kuppusamy, P., Zewier, Z.L., Arancio, O., Stern, D., Yan, S.S., Wu, H., 2004. ABAD directly links Abeta to mitochondrial toxicity in Alzheimer's disease. Science 304, 448–452.
Maalouf, M., Rho, J.M., 2008. Oxidative impairment of hippocampal long-term potentiation involves activation of protein phosphatase 2A and is prevented by ketone bodies. J. Neurosci. Res. 86, 3322–3330.
Mayeux, R., Stern, Y., 2012. Epidemiology of Alzheimer disease. Cold Spring Harbor Perspect. Med. 2, 1–18.
Mc Donald, J.M., Savva, G.M., Brayne, C., Welzel, A.T., Forster, G., Shankar, G.M., Selkoe, D.J., Ince, P.G., Walsh, D.M., 2010. The presence of sodium dodecyl sulphate-stable Abeta dimers is strongly associated with Alzheimer-type dementia. Brain 133 (Pt 5), 1328–1341.
Mucke, L., Masliah, E., Yu, G.Q., Mallory, M., Rockenstein, E.M., Tatsuno, G., Hu, K., Kholodenko, D., Johnson-Wood, K., McConlogue, L., 2000. High-level neuronal expression of abeta 1-42 in wild-type human amyloid protein precursor transgenic mice: synaptotoxicity without plaque formation. J. Neurosci. 20, 4050–4058.
Mucke, L., Selkoe, D.J., 2012. Neurotoxicity of amyloid β-protein: synaptic and network dysfunction. Cold Spring Harbor Perspect. Med. 2, a006338.
Murphy, M.P., 2009. How mitochondria produce reactive oxygen species. Biochem. J. 417, 1–13.
Newman, J.C., Verdin, E., 2014. Beta-hydroxybutyrate: much more than a metabolite. Diabetes Res. Clin. Pract. 106, 173–181.
Newport, M.T., VanItallie, T.B., Kashiwaya, Y., King, M.T., Veech, R.L., 2015. A new way to produce hyperketonemia: use of ketone ester in a case of Alzheimer's disease. Alzheimers Dement. 11, 99–103.
Payne, N.E., Cross, J.H., Sander, J.W., Sisodiya, S.M., 2011. The ketogenic and related diets in adolescents and adults—a review. Epilepsia 52, 1941–1948.
Pujadas, L., Rossi, D., Andres, R., Teixeira, C.M., Serra-Vidal, B., Parcerisas, A., Maldonado, R., Giralt, E., Carulla, N., Soriano, E., 2014. Reelin delays amyloid-beta fibril formation and rescues cognitive deficits in a model of Alzheimer's disease. Nat. Commun. 5, 3443.
Quist, A., Doudevski, I., Lin, H., Azimova, R., Ng, D., Frangione, B., Kagan, B., Ghiso, J., Lal, R., 2005. Amyloid ion channels: a common structural link for protein-misfolding disease. Proc. Natl. Acad. Sci. U. S. A. 102, 10427–10432.
Rahman, M., Muhammad, S., Khan, M.A., Chen, H., Ridder, D.A., Muller-Fielitz, H., Pokorna, B., Vollbrandt, T., Stolting, I., Nadrowitz, R., Okun, J.G., Offermanns, S., Schwaninger, M., 2014. The beta-hydroxybutyrate receptor HCA2 activates a neuroprotective subset of macrophages. Nat. Commun. 5, 3944.
Rinetti, G.V., Schweizer, F.E., 2010. Ubiquitination acutely regulates presynaptic neurotransmitter release in mammalian neurons. J. Neurosci. 30, 3157–3166.
Roberson, E.D., Scearce-Levie, K., Palop, J.J., Yan, F., Cheng, I.H., Wu, T., Gerstein, H., Yu, G.Q., Mucke, L., 2007. Reducing endogenous tau ameliorates amyloid beta-induced deficits in an Alzheimer's disease mouse model. Science 316, 750–754.
Schneider, C.A., Rasband, W.S., Eliceiri, K.W., 2012. NIH Image to ImageJ: 25 years of image analysis. Nat. Methods 9, 671–675.
Sepulveda, F.J., Fierro, H., Fernandez, E., Castillo, C., Peoples, R.W., Opazo, C., Aguayo, L.G., 2014. Nature of the neurotoxic membrane actions of amyloid-beta on hippocampal neurons in Alzheimer's disease. Neurobiol. Aging 35, 472–481.
Seyfried, T.N., Mukherjee, P., 2005. Targeting energy metabolism in brain cancer: review and hypothesis. Nutr. Metab. 2, 30.
Shimazu, T., Hirschey, M.D., Newman, J., He, W., Shirakawa, K., Le Moan, N., Grueter, C.A., Lim, H., Saunders, L.R., Stevens, R.D., Newgard, C.B., Farese Jr., R.V., de Cabo, R., Ulrich, S., Akassoglou, K., Verdin, E., 2013. Suppression of oxidative stress by beta-hydroxybutyrate, an endogenous histone deacetylase inhibitor. Science 339, 211–214.
Song, H.L., Shim, S., Kim, D.H., Won, S.H., Joo, S., Kim, S., Jeon, N.L., Yoon, S.Y., 2014. Beta-amyloid is transmitted via neuronal connections along axonal membranes. Ann. Neurol. 75, 88–97.
Szatmari, E.M., Oliveira, A.F., Sumner, E.J., Yasuda, R., 2013. Centaurin-alpha1-Ras-Elk-1 signaling at mitochondria mediates beta-amyloid-induced synaptic dysfunction. J. Neurosci. 33, 5367–5374.
Terwel, D., Steffensen, K.R., Verghese, P.B., Kummer, M.P., Gustafsson, J.A., Holtzman, D.M., Heneka, M.T., 2011. Critical role of astroglial apolipoprotein E and liver X receptor-alpha expression for microglial Abeta phagocytosis. J. Neurosci. 31, 7049–7059.
Thaipisuttikul, P., Galvin, J.E., 2012. Use of medical foods and nutritional approaches in the treatment of Alzheimer's disease. Clin. Pract. (Lond) 9, 199–209.
Umeda, T., Tomiyama, T., Sakama, N., Tanaka, S., Lambert, M.P., Klein, W.L., Mori, H., 2011. Intraneuronal amyloid beta oligomers cause cell death via endoplasmic reticulum stress, endosomal/lysosomal leakage, and mitochondrial dysfunction in vivo. J. Neurosci. Res. 89, 1031–1042.
Wang, X., Wang, W., Li, L., Perry, G., Lee, H.G., Zhu, X., 2013. Oxidative stress and mitochondrial dysfunction in Alzheimer's disease. Biochim. Biophys. Acta 1842, 1240–1247.
Yin, J., Turner, G.H., Coons, S.W., Maalouf, M., Reiman, E.M., Shi, J., 2014. Association of amyloid burden, brain atrophy and memory deficits in aged apolipoprotein epsilon4 mice. Curr. Alzheimer Res. 11, 283–290.
Yin, J.X., Turner, G.H., Lin, H.-j., Coons, S.W., Shi, J., 2011. Deficits in spatial learning and memory is associated with hippocampal volume loss in aged apolipoprotein E4 mice. J. Alzheimer's Dis. 27, 89–98.